

Lawrence Berkeley National Laboratory

Recent Work

Title

Observation of a Luttinger-liquid plasmon in metallic single-walled carbon nanotubes

Permalink

<https://escholarship.org/uc/item/8338c3w4>

Journal

Nature Photonics, 9(8)

ISSN

1749-4885

Authors

Shi, Z
Hong, X
Bechtel, HA
[et al.](#)

Publication Date

2015-07-20

DOI

10.1038/nphoton.2015.123

Peer reviewed

Observation of Luttinger-liquid plasmon in metallic single-walled carbon nanotubes

Zhiwen Shi^{1*†}, Xiaoping Hong^{1*}, Hans A. Bechtel², Bo Zeng¹, Michael C. Martin², Kenji Watanabe³, Takashi Taniguchi³, Yuen-Ron Shen^{1,4}, Feng Wang^{1,4,5†}

¹Department of Physics, University of California at Berkeley, Berkeley, California 94720, USA.

²Advanced Light Source Division, Lawrence Berkeley National Laboratory, Berkeley, California 94720, USA.

³Advanced Materials Laboratory, National Institute for Materials Science, 1-1 Namiki, Tsukuba, 305-0044, Japan.

⁴Materials Science Division, Lawrence Berkeley National Laboratory, Berkeley, California 94720, USA.

⁵Kavli Energy NanoSciences Institute at the University of California, Berkeley and the Lawrence Berkeley National Laboratory, Berkeley, California, 94720, USA.

*These authors contributed equally to this work.

†To whom correspondence should be addressed. Email: fengwang76@berkeley.edu,

zhiwen22@gmail.com

Surface plasmons¹, collective oscillations of conduction electrons, hold great promise for nanoscale integration of photonics and electronics¹⁻⁴. However, nanophotonic circuits based on plasmons have been significantly hampered by the difficulty in achieving broadband plasmonic waveguides that exhibit simultaneously strong spatial confinement, high quality factor, and low dispersion. Quantum plasmons, where quantum mechanical effects of electrons play a dominant role, such as plasmons in very small metal nanoparticles^{5,6} and plasmons affected by tunneling effects⁷, can lead to novel plasmonic phenomena in nanostructures. Here we show that Luttinger liquid^{8,9} of one-dimensional Dirac electrons in carbon nanotubes¹⁰⁻¹³ exhibit quantum plasmons that behave qualitatively different from classical plasmon excitations: the Luttinger-liquid plasmon propagates at “quantized” velocities that are independent of carrier concentration or excitation wavelength, and they exhibit extraordinary spatial confinement and a high quality factor simultaneously. Such Luttinger-liquid plasmons could enable novel low-loss plasmonic circuits for the sub-wavelength manipulation of light.

Quantum-confined electrons in one dimension (1D) behave as Luttinger liquid, a strongly correlated electronic matter distinctly different from quasi-free electrons described by the Fermi liquid^{8,9}. A defining characteristic of the Luttinger liquid is the spin-charge separation, where the spin and charge excitations propagate at different speeds. The elementary charge excitations of the Luttinger liquid are 1D quantum plasmons, which are distinctly different from their classical counterparts: classically plasmons are determined by the free electron density and effective mass as in Drude conductivity. This description completely breaks down for Luttinger-liquid plasmons, which are instead determined by the electron Fermi velocity and the number of quantum conducting channels^{10,11}. Metallic single-walled carbon nanotubes (SWNTs), with their extraordinary 1D quantum confinement, provide the ideal platform to explore such Luttinger-liquid plasmons. Due to strong quantum confinement, Luttinger-liquid plasmons in SWNTs of 1 nm diameter should persist to visible frequencies before the first inter-subband transition appears¹⁴. In addition, the forbidden backscattering of Dirac electrons^{15,16}, evidenced by ballistic transport up to micron lengths¹⁷⁻¹⁹ in metallic SWNTs, can lead to strongly confined but low loss Luttinger-liquid plasmons. However, the experimental observation of such Luttinger liquid plasmons in SWNTs has remained an outstanding challenge for over a decade, although previous electrical transport and photoemission measurements have shown the presence of Luttinger liquid in SWNTs^{12,13,20}.

Here we report the first observation of Luttinger-liquid plasmons in SWNTs using infrared (IR) scattering-type scanning near-field optical microscopy (s-SNOM)²¹⁻²³. We show that the Luttinger liquid plasmons can be excited in a broad

frequency range, and they propagate at a “quantized” velocity in individual SWNTs. This velocity, unlike classical plasmon oscillations, does not depend on the free carrier density, and varies only weakly with the plasmon frequency or nanotube diameter. Instead, it is mainly determined by the quantized number of conducting channels in SWNTs. At the same time, Luttinger-liquid plasmons in SWNTs exhibit strong spatial confinement and high-quality factor simultaneously, a most sought-after feature in plasmonics²⁴. Our observed quantum plasmon behavior agrees quantitatively with the Luttinger liquid theory of nanotubes. Such Luttinger-liquid plasmons in SWNTs holds great potential for novel broadband plasmonic waveguides and nanophotonic circuits with low dispersion, high quality factor, and strong subwavelength confinement.

Metallic SWNTs with diameter from 1.2 nm to 1.7 nm were grown by the arc-discharge method, which were then suspended in a micelle solution using ultrasonication and purified to 95% metallic SWNTs using density gradient ultracentrifugation²⁵. Afterwards, the nanotube solution was spin-coated onto thin hexagonal boron nitride (BN) flakes on SiO₂/Si substrates to yield isolated individual and small bundles of SWNTs. Here we choose BN as substrates because BN is atomically flat and extremely clean, which facilitates the observation of Luttinger liquid plasmon in nanotubes. In contrast, it is very difficult to observe plasmon excitation in nanotubes spin-coated directly on SiO₂/Si substrates. Plasmons in these metallic SWNTs are probed using IR s-SNOM, as illustrated in Fig. 1a. Infrared light at 6.1 μm or 10.6 μm is focused onto the apex of a metal-coated atomic force microscope (AFM) tip with a curvature radius $r \approx 25$ nm, the large

near-field momentum of which enables optical excitation of plasmons in SWNTs. The excited plasmon wave propagates along the SWNT and is reflected at the nanotube end. The back-reflected plasmon wave interferes with the excitation wave underneath the tip, which modifies the intensity of tip-scattered IR radiation measured by an HgCdTe detector in the far field. As the tip is scanned along the nanotube, the scattered IR radiation varies periodically, with intensity peaks appearing at positions of constructive interference^{23,26,27}. Figure 1b displays a representative IR s-SNOM image of a metallic SWNT, the topography of which is recorded simultaneously (shown in the inset). Prominent plasmon oscillation along the whole length of the nanotube can be clearly observed in ambient conditions.

We systematically investigated plasmons in different SWNTs on BN substrates. The nanotubes spin-coated on BN were first characterized by a recently developed in-situ single tube spectroscopy²⁸. Figure 2a and 2b show optical spectra of two representative individual SWNTs, which are characterized by one or two prominent optical resonances. From these resonances, we can identify the nanotube chirality to be (11, 11) and (15, 6)¹⁴, corresponding to metallic nanotubes with diameters of 1.49 nm and 1.47 nm, respectively. Figure 2c displays the optical spectrum of a typical small bundle, which is characterized by broader optical features and more resonances. We found that the spin-coated nanotubes are either individual SWNTs or small bundles, and almost all individual SWNTs are metallic, consistent with the high metallic nanotube percentage in these samples.

Figure 2d-2g show four AFM topography images of SWNTs on BN substrates, and Fig. 2h-2k display the corresponding near-field IR s-SNOM images of 1D

plasmons in these nanotubes with 10.6 μm or 6.1 μm photon excitation. Periodic oscillation of the tip-induced IR scattering from 1D Luttinger-liquid plasmons is apparent in all nanotubes. The oscillation period, however, varies for different IR excitation wavelengths and in different nanotubes. Figure 2h and 2i show near-field IR scattering images with 10.6 μm and 6.1 μm excitation, respectively, for the same nanotube. The oscillation period is longer for 10.6 μm excitation, and the oscillation period and the excitation wavelength have almost the same ratio, consistent with a linear scaling. Figure 2i-2k display near-field IR scattering images in different nanotubes. Fig. 2k shows clearly that the oscillation period becomes longer in a bundle than those in the constituent nanotubes. Next, we determine the Luttinger-liquid plasmon wavelength and propagation velocity in different nanotube samples. The scattering peaks in the IR s-SNOM images (Fig. 2h-2k) are determined by constructive interference where the reflected plasmon accumulates a phase change $\Delta\varphi = 2 \cdot 2\pi L/\lambda_p + \varphi_0 = 2m\pi$. Here L is the distance between the tip and tube end, λ_p is the plasmon wavelength, φ_0 is the reflection phase change, and m is an integer. Therefore the plasmon wavelength λ_p is simply twice the oscillation period observed in the IR s-SNOM images. The propagation velocity of a 1D plasmon (v_p) can be readily calculated from its frequency and wavelength by $v_p = \nu \cdot \lambda_p = c \cdot \lambda_p/\lambda_0$, where ν is the frequency, c is the speed of light, and λ_0 is the free-space photon wavelength.

We plot in Fig. 3a and Fig. 3b the plasmon wavelength (λ_p , left axis) and the corresponding plasmon velocity (v_p/v_F , right axis) in different nanotubes with 10.6 μm and 6.1 μm excitation, respectively. We found that the plasmon velocity exhibits

a quantized behavior: among 22 measured nanotubes with 10.6 μm excitation, 10 tubes have a plasmon velocity “quantized” at a minimum value of $3.2 v_F$, another 7 nanotubes have v_p clustered around $4.4 v_F$, and the others have v_p of $5.3 v_F$ and $6.2 v_F$. These “quantized” velocities can be well approximated by a simple ratio of $1:\sqrt{2}:\sqrt{3}:\sqrt{4}$. Similar “quantized” velocities are also observed for 6.1 μm excitation, although the absolute values are slightly larger. Such “quantized” plasmon propagation velocities in as-prepared nanotubes, which have different diameters and carrier concentrations from environmental doping, is qualitatively different from the behavior of classical plasmons.

To understand the unusual propagation of Luttinger-liquid plasmons, we examine quantitatively the Luttinger liquid behavior in individual and small bundles of metallic SWNTs. The pioneering work by Kane et al. shows that interacting electrons in metallic SWNTs are described by strongly renormalized Luttinger liquid¹⁰. This Luttinger liquid in SWNTs is fully characterized by the Luttinger liquid parameter g describing the type and strength of the interaction. Non-interacting electron gases are described by $g=1$, while attractive interactions have $g>1$ and repulsive interactions have $g<1$. The plasmon velocity v_p is related to g simply by $v_p=v_F/g$. For individual suspended SWNTs of radius R screened by a concentric metal shell of radius R_s , the Luttinger liquid parameter can be calculated quantitatively as $1/g=\sqrt{1 + (8e^2/\pi\hbar v_F)\ln(R_s/R)}$, where the second term arises from long-range Coulomb interactions and is proportional to the number of conducting channels and the unit length capacitance between the coaxial nanotube and metal shell¹⁰. For plasmons in small nanotube bundles residing on a substrate,

the Coulomb interaction term is modified, and the Luttinger liquid parameter becomes

$$1/g = v_p/v_F \approx \sqrt{1 + (2 \times 4Ne^2/\epsilon_{eff}\pi\hbar v_F)\ln(\lambda_p/2\pi R_t)}, \quad (1)$$

where N is the number of SWNTs in a bundle and $4N$ is the number of quantized conducting channels, ϵ_{eff} is the effective dielectric constant due to the substrate screening, R_t is the effective radius of the nanotube bundle, and the plasmon wavelength λ_p determines the cut-off length of Coulomb interactions. (See supplementary information for details.)

The Luttinger liquid theory indeed predicts very unusual plasmon propagation velocities. Unlike classical plasmon excitations, the Luttinger-liquid plasmon velocity in Eq. 1 does not depend on the electron density at all. Instead, it is mainly determined by the quantized number of conducting channels $4N$. The plasmon velocity varies with R_t and λ_p only weakly in a logarithmical fashion. The theory accounts for our observed quantization of the plasmon propagation speed: plasmons travels at the velocities with a ratio around $1:\sqrt{2}:\sqrt{3}:\sqrt{4}$ for individual SWNTs and bundles containing 2, 3, and 4 tubes; and nanotubes with different diameters and carrier density have almost the same plasmon velocity. More quantitatively, we calculated the predicted range of plasmon velocities for N -tube bundles using Eq. 1 and plot them in Fig. 3 (shaded areas). Here we have included the tube diameter distribution between 1.2 nm and 1.7 nm, approximated the effective radius of a nanotube bundle as \sqrt{NR} , and used an effective dielectric constant $\epsilon_{eff}=2.1$ at 10.6 μm and $\epsilon_{eff}=1.0$ at 6.1 μm due to dielectric screening from the BN substrates (See the supplementary information for more details). This

Luttinger liquid theory, which is free of adjustable parameters, matches quantitatively with the experimental data. We note that although the plasmon frequency at 6.1 μm is almost twice of that at 10.6 μm , the plasmon velocity changes only 15% and it is largely due to the frequency-dependent BN dielectric constant. It highlights the low dispersion of Luttinger-liquid plasmons in SWNTs.

Luttinger-liquid plasmons in metallic SWNTs also exhibit a remarkable combination of strong spatial confinement and high quality factors, two key figures of merit for plasmonics²⁴. The Luttinger-liquid plasmons are characterized by extraordinary sub-wavelength confinement. The plasmon wavelength along the nanotube is as small as 1/100 of the free-space light wavelength (Fig. 3 and insets of Fig. 4a and 4b). The transverse confinement is even stronger: Figure 4c shows the numerically simulated transverse electrical field distribution of the 1D plasmon in a SWNT, which shows a spatial confinement of $\sim 1\text{nm}$, less than 1/1000 of $\lambda_0 = 10.6 \mu\text{m}$. Strikingly, such strongly confined 1D plasmon can propagate over a long distance with little attenuation in SWNTs. Figure 4a and 4b display the oscillating IR scattering intensity along two different nanotubes (black lines). We can estimate the quality factor Q of the corresponding 1D plasmon by fitting the oscillation with an exponential decay of the form $e^{-2\pi x/(Q \cdot \lambda_p)} \sin(\frac{4\pi x}{\lambda_p})$ from the nanotube end (red line in Fig. 4a and 4b). Although fitting over the whole nanotube is difficult due to fluctuations in the near-field IR scattering intensity, good agreement can be obtained for clean oscillations near the end of a nanotube, which yields a quality factor over 20 in SWNTs shown in Fig. 4a and 4b. This combination of extraordinary spatial confinement ($\lambda_p/\lambda_0 \sim 1/100$) and high quality factor ($Q > 20$) in nanotube

plasmon is unprecedented. Typically, a strong spatial confinement of plasmon can only be achieved at the expense of a low quality factor due to the absorption loss of metals. For instance, a two-dimensional (2D) surface plasmon at the silver/air interface has a quality factor $Q \sim 16$ with $\lambda_p/\lambda_0 = 1.16$ at 400 nm, but Q worsens to ~ 2.27 when λ_p/λ_0 increases to 1.51 at 350 nm²⁹. Similarly, 2D plasmons in graphene can have rather good spatial confinement ($\lambda_p/\lambda_0 \sim 1/50$), but the quality factor Q is limited to ~ 5 ^{26,27}.

The remarkably low loss of Luttinger-liquid plasmon in SWNTs presumably originates from the unique properties of 1D chiral electrons in carbon nanotubes. Electrons in metallic SWNTs are described by relativistic Dirac fermions, where forward and backward moving electrons have opposite chiral handedness. Such chiral electrons cannot be backscattered by slowly varying charge impurity potential or acoustic phonons because the electron handedness has to be preserved (Fig. 4d)^{15,16,30}. The protection from backscattering eliminates all loss channels in 1D SWNTs. This is in contrast to 2D graphene, where Dirac electrons can still be scattered to angles different from 180 degrees even with forbidden backscattering. The lack of electron backscattering in SWNTs leads to very long electron mean free path in electrical transport even for nanotubes on SiO₂/Si substrates at room temperature^{18,19}. Here it gives rise to Luttinger liquid plasmons with low absorption loss and long-range propagation although the spatial confinement is strongly subwavelength.

Our direct observation of Luttinger-liquid plasmons opens up exciting new opportunities to explore both 1D Luttinger liquid physics and quantum plasmons in

carbon nanotubes, the properties of which can be manipulated through electrostatic gating, mechanical strain, and external magnetic field. Although our studies focused on Luttinger-liquid plasmon at infrared wavelengths, the Luttinger liquid behavior in SWNTs should be valid over a broad frequency range up to visible frequencies because the first inter-subband transition is above 1.7 eV for metallic nanotubes of 1.5 nm diameter (Fig. 2a, b) due to strong quantum confinement in SWNTs¹⁴. The combination of low dispersion, high quality factor, and strong subwavelength confinement in Luttinger-liquid plasmon holds great potential for novel plasmonic and nanophotonic devices over a broad frequency range, including telecom wavelengths.

References:

- 1 Barnes, W. L., Dereux, A. & Ebbesen, T. W. Surface plasmon subwavelength optics. *Nature* **424**, 824-830 (2003).
- 2 Gramotnev, D. K. & Bozhevolnyi, S. I. Plasmonics beyond the diffraction limit. *Nature Photonics* **4**, 83-91 (2010).
- 3 Schuller, J. A. *et al.* Plasmonics for extreme light concentration and manipulation. *Nature Materials* **9**, 193-204 (2010).
- 4 Pendry, J. B., Aubry, A., Smith, D. R. & Maier, S. A. Transformation Optics and Subwavelength Control of Light. *Science* **337**, 549-552 (2012).
- 5 Halperin, W. P. Quantum Size Effects in Metal Particles. *Reviews of Modern Physics* **58**, 533-606 (1986).
- 6 Scholl, J. A., Koh, A. L. & Dionne, J. A. Quantum plasmon resonances of individual metallic nanoparticles. *Nature* **483**, 421-U468 (2012).
- 7 Tan, S. F. *et al.* Quantum Plasmon Resonances Controlled by Molecular Tunnel Junctions. *Science* **343**, 1496-1499 (2014).
- 8 Luttinger, J. M. An Exactly Soluble Model of a Many-Fermion System. *J Math Phys* **4**, 1154 (1963).
- 9 Voit, J. One-Dimensional Fermi Liquids. *Reports on Progress in Physics* **58**, 977-1116 (1995).
- 10 Kane, C., Balents, L. & Fisher, M. P. A. Coulomb interactions and mesoscopic effects in carbon nanotubes. *Physical Review Letters* **79**, 5086-5089 (1997).
- 11 Egger, R. & Gogolin, A. O. Effective low-energy theory for correlated carbon nanotubes. *Physical Review Letters* **79**, 5082-5085 (1997).

- 12 Bockrath, M. *et al.* Luttinger-liquid behaviour in carbon nanotubes. *Nature* **397**, 598-601 (1999).
- 13 Yao, Z., Postma, H. W. C., Balents, L. & Dekker, C. Carbon nanotube intramolecular junctions. *Nature* **402**, 273-276 (1999).
- 14 Liu, K. *et al.* An atlas of carbon nanotube optical transitions. *Nat. Nanotechnol.* **7**, 325-329 (2012).
- 15 Ando, T., Nakanishi, T. & Saito, R. Berry's phase and absence of back scattering in carbon nanotubes. *J. Phys. Soc. Jpn.* **67**, 2857-2862 (1998).
- 16 McEuen, P. L., Bockrath, M., Cobden, D. H., Yoon, Y. G. & Louie, S. G. Disorder, pseudospins, and backscattering in carbon nanotubes. *Physical Review Letters* **83**, 5098-5101 (1999).
- 17 Javey, A., Guo, J., Wang, Q., Lundstrom, M. & Dai, H. J. Ballistic carbon nanotube field-effect transistors. *Nature* **424**, 654-657 (2003).
- 18 Park, J. Y. *et al.* Electron-phonon scattering in metallic single-walled carbon nanotubes. *Nano Letters* **4**, 517-520 (2004).
- 19 Purewal, M. S. *et al.* Scaling of resistance and electron mean free path of single-walled carbon nanotubes. *Physical Review Letters* **98**, 186808 (2007).
- 20 Ishii, H. *et al.* Direct observation of Tomonaga-Luttinger-liquid state in carbon nanotubes at low temperatures. *Nature* **426**, 540-544 (2003).
- 21 Hillenbrand, R., Knoll, B. & Keilmann, F. Pure optical contrast in scattering-type scanning near-field microscopy. *J Microsc-Oxford* **202**, 77-83 (2001).
- 22 Bechtel, H. A., Muller, E. A., Olmon, R. L., Martin, M. C. & Raschke, M. B. Ultrabroadband infrared nanospectroscopic imaging. *Proceedings of the National Academy of Sciences of the United States of America* **111**, 7191-7196 (2014).
- 23 Gerber, J. A., Berweger, S., O'Callahan, B. T. & Raschke, M. B. Phase-Resolved Surface Plasmon Interferometry of Graphene. *Physical Review Letters* **113**, 055502 (2014).
- 24 Boltasseva, A. & Atwater, H. A. Low-Loss Plasmonic Metamaterials. *Science* **331**, 290-291 (2011).
- 25 Arnold, M. S., Green, A. A., Hulvat, J. F., Stupp, S. I. & Hersam, M. C. Sorting carbon nanotubes by electronic structure using density differentiation. *Nat. Nanotechnol.* **1**, 60-65 (2006).
- 26 Fei, Z. *et al.* Gate-tuning of graphene plasmons revealed by infrared nano-imaging. *Nature* **487**, 82-85 (2012).
- 27 Chen, J. *et al.* Optical nano-imaging of gate-tunable graphene plasmons. *Nature* **487**, 77-81 (2012).
- 28 Liu, K. H. *et al.* High-throughput optical imaging and spectroscopy of individual carbon nanotubes in devices. *Nat. Nanotechnol.* **8**, 917-922 (2013).
- 29 Palik, E. D. *Handbook of Optical Constants of Solids.* (Elsevier, 1997).
- 30 Suzuura, H. & Ando, T. Phonons and electron-phonon scattering in carbon nanotubes. *Physical Review B* **65**, 235412 (2002).

Acknowledgements: We thank Markus Raschke for helpful discussions. H.B. and M.M., in particular, thank Raschke and his group for the years of pioneering research on IR near-field techniques and key collaborations that led to the development of a near-field IR instrument at the Advanced Light Source (ALS). We also thank Kaihui Liu, Yinghui Sun, Sufei Shi, Chenhao Jin and Henry Chang for their help on sample preparation and helpful discussions. This work was primarily supported by Office of Basic Energy Science, Department of Energy under contract No. DE-AC02-05CH11231 (Sub-wavelength Metamaterial program) and DE-SC0003949 (Early Career Award). Spectroscopy of nanotubes in the visible range was supported by the National Science Foundation grant No. DMR-1404865. The Advanced Light Source is supported by the Director, Office of Science, Office of Basic Energy Sciences, of the U.S. Department of Energy under Contract No. DE-AC02-05CH11231. F.W. acknowledges the support from a David and Lucile Packard fellowship.

Author contributions: F.W. and Z.S. conceived the project. Z.S. and X.H. prepared the nanotube samples. Z.S. and H.B. performed the near-field IR measurements, X.H. and Z.B. performed visible spectroscopy. X.H., Z.S. and F.W. analyzed the data. All authors discussed the results and contributed to writing the manuscript.

Additional information: Supplementary information is available in the online version of the paper. Reprints and permissions information is available online at www.nature.com/reprints. Correspondence and requests for materials should be addressed to F.W. or Z.S.

Figure captions:

Figure 1 Infrared s-SNOM of one-dimensional plasmons in carbon nanotubes.

a, Illustration of the scattering-type scanning near-field optical microscopy (s-SNOM). Infrared (IR) light is focused onto the apex of a metal-coated atomic force microscope (AFM) tip, the large near-field momentum of which enables optical excitation of plasmons in the carbon nanotube (CNT) on a boron nitride (BN) substrate. The interference between the tip excited plasmon wave and its reflection from nanotube end leads to periodic modulation of tip-scattered IR radiation measured by an HgCdTe detector in the far field. **b**, A three-dimensional plot of the near-field scattering intensity (height) along a representative SWNT. Prominent modulation of the IR scattering intensity from the 1D plasmon can be observed over the whole nanotube. The inset displays the AFM topography image of the same SWNT. Scale bar is 100 nm.

Figure 2 Luttinger-liquid plasmons in carbon nanotubes. **a**, **b** and **c**, Optical spectra (black) of individual metallic SWNTs with chirality of (11,11) **a** and (15,6) **b**, and of a small nanotube bundle **c**. The red curves are guiding lines. **d-g**, AFM topography images of representative nanotube samples. **h-k**, IR s-SNOM images with different excitation wavelengths for tubes shown in **d-g**. **h** and **i** display near-field IR images for the same nanotube with 10.6 μm and 6.1 μm excitation, respectively. The IR scattering oscillation period is consistent with a linear scaling behavior with excitation wavelength. **i**, **j**, **k** show the IR scattering oscillation in different nanotubes with 6.1 μm excitation. In particular, **k** reveals that the

oscillation period gets longer when tubes coalesce into bigger bundles. Scale bar: 100 nm.

Figure 3 Quantized Luttinger-liquid plasmon propagation velocity. The plasmon wavelength λ_p (left axis) and propagation velocity v_p/v_F (or $1/g$, right axis) for different nanotubes with 10.6 μm (**a**) and 6.1 μm (**b**) excitation. The Luttinger-liquid plasmon shows quantization propagation velocities around a few discrete values, which can be approximated by a simple ratio of $1:\sqrt{2}:\sqrt{3}:\sqrt{4}$ that are related to the quantized number of conducting channels in different nanotubes. The experimental data agrees well with the Luttinger liquid theory (shaded ribbons), where we have included the effects of a finite SWNT diameter distribution (1.2-1.7 nm) and an effective dielectric constant of 2.1 for 10.6 μm and 1.0 for 6.1 μm from the substrate screening. Error bars represent the uncertainty from fitting the 1D plasmon profiles.

Figure 4 Long-range quantum plasmons in nanotubes. **a** and **b**, Oscillation of near-field IR scattering intensity from 1D plasmons in two metallic nanotubes. Fitting of the oscillation near the nanotube end yields a plasmon quality factor Q over 20 in both SWNTs, although the plasmon wavelength λ_p is only $\sim 1/100$ of the free space wavelength λ_0 . **c**, Numerical simulation of the electrical field distribution of the 1D plasmon around a nanotube of 2nm diameter, which shows a transverse confinement of the electrical field within a few nanometers, less than $1/1000$ of λ_0 . Scale bar: 1nm. **d**, Illustration of the chirality of Dirac electrons in SWNTs, where

left and right moving electrons are characterized by opposite pseudo-spins. Backscattering is forbidden for such Dirac electrons, and it leads to the remarkably low loss of 1D nanotube plasmon even with the strong spatial confinement.

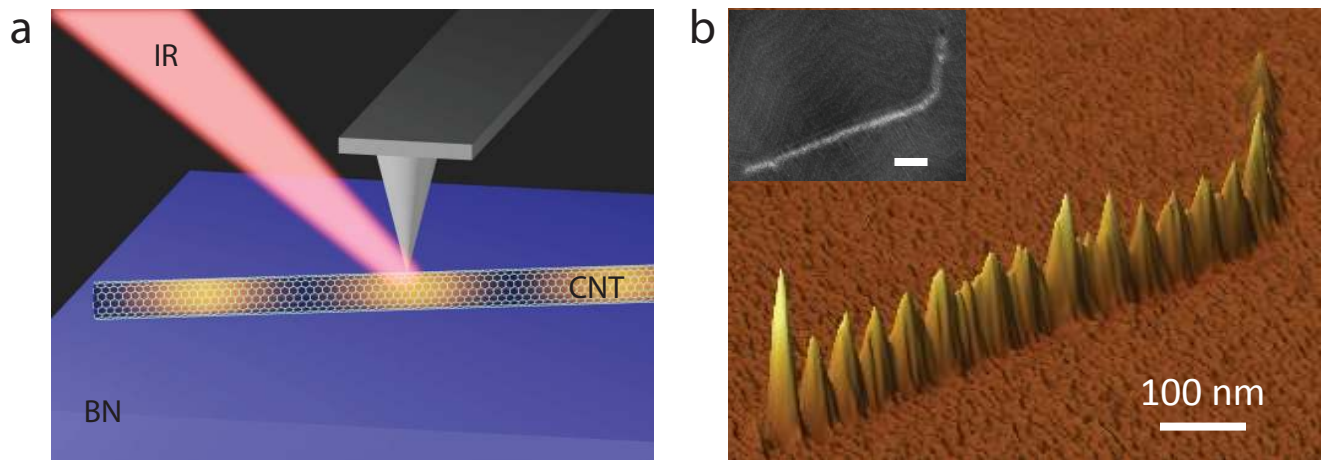


Figure 1

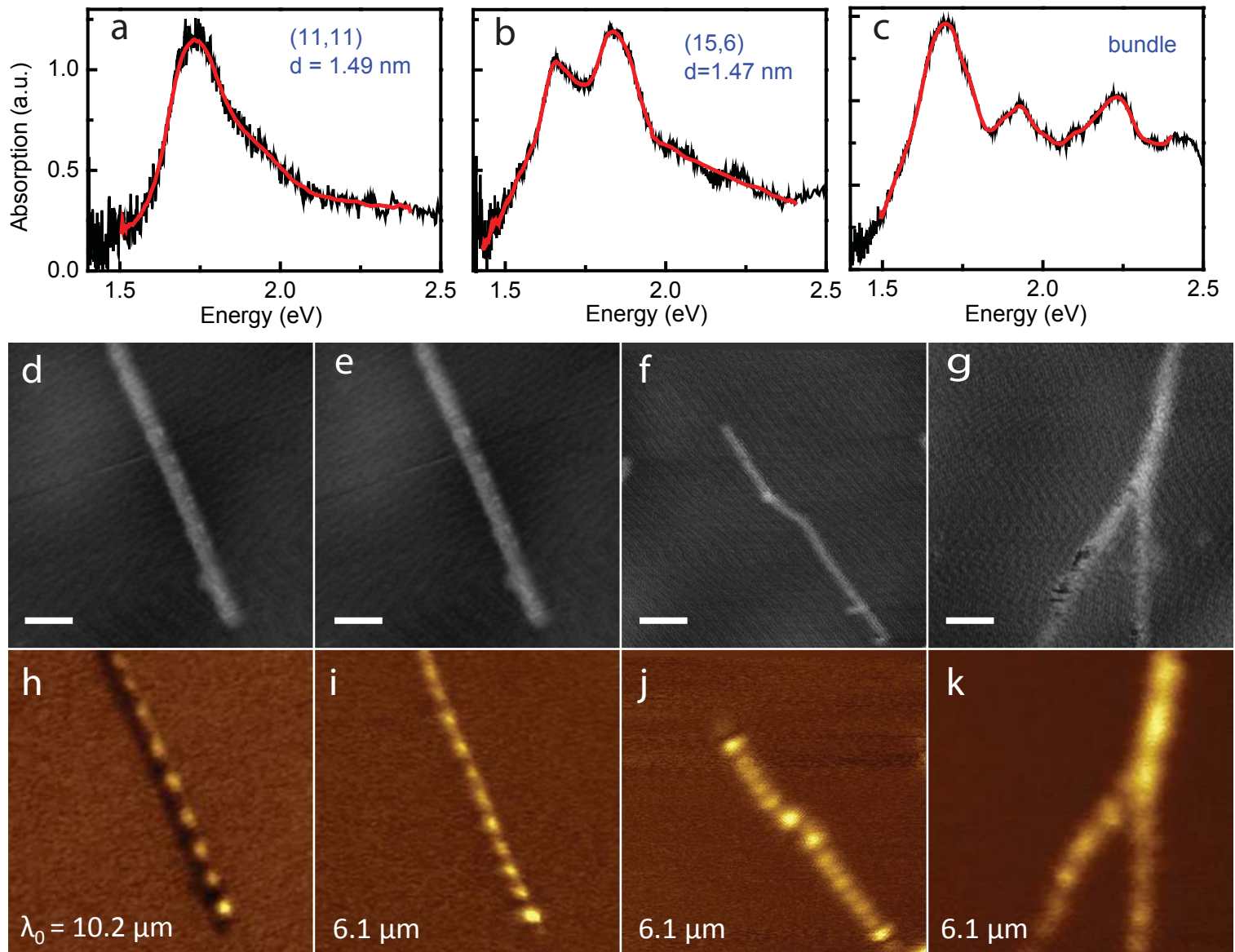


Figure 2

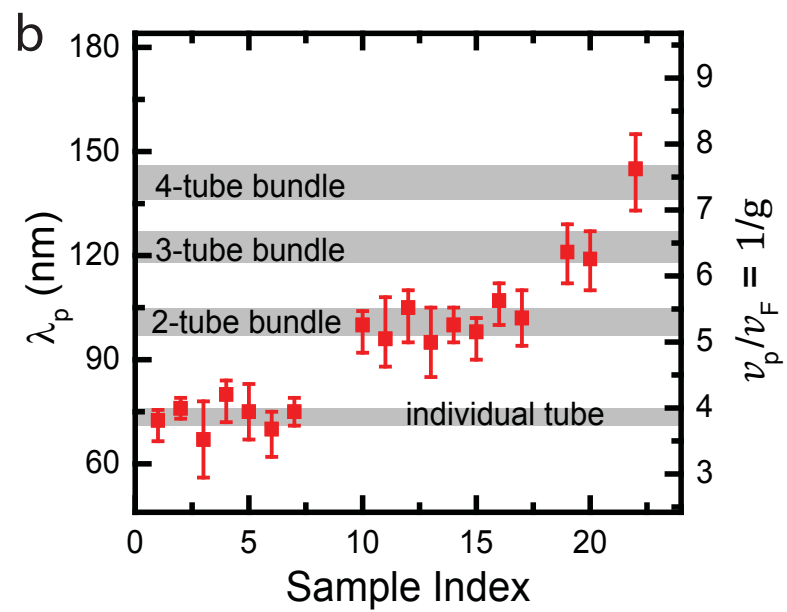
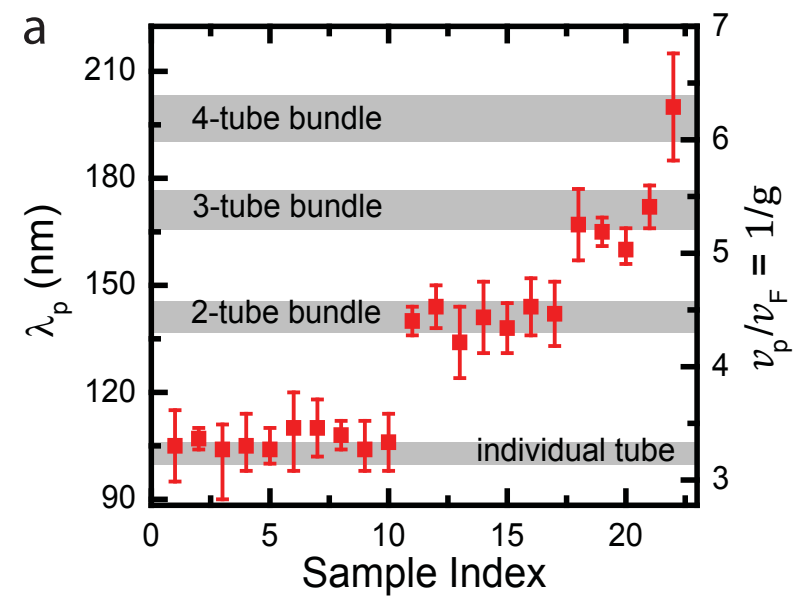


Figure 3

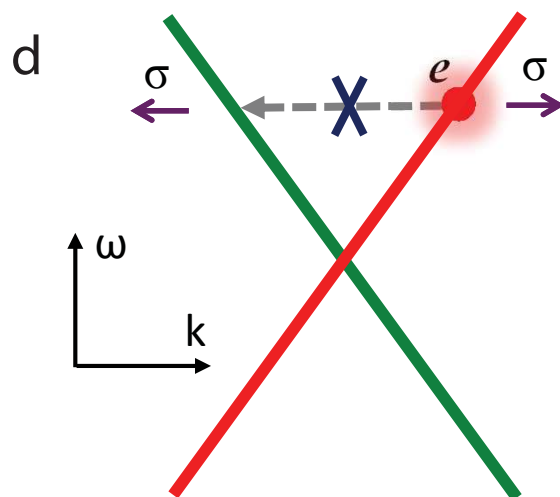
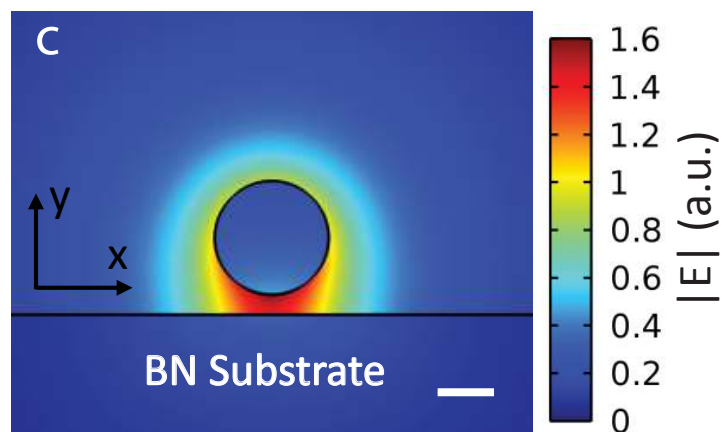
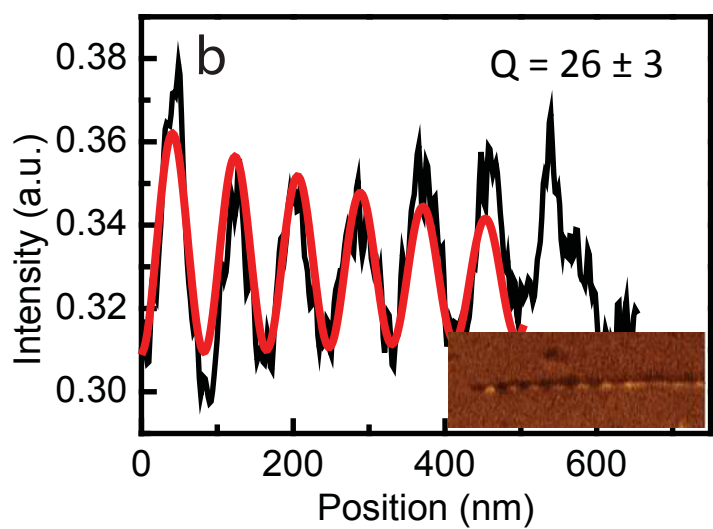
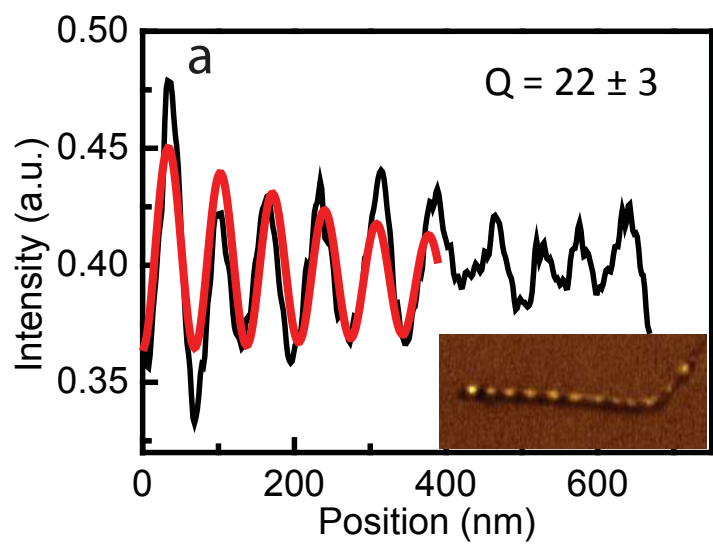


Figure 4